

Comparisons of Air Radiation Model with Shock Tube Measurements

Deepak Bose¹,
NASA Ames Research Center, Moffett Field, CA 94035, USA

Evan McCorkle²,
North Carolina State University, Raleigh, NC 27695

and
David Bogdanoff³, and Gary A. Allen, Jr.³
ELORET Corporation, NASA Ames Research Center, Moffett Field, CA 94035, USA

Abstract

This paper presents an assessment of the predictive capability of shock layer radiation model appropriate for NASA's Orion Crew Exploration Vehicle lunar return entry. A detailed set of spectrally resolved radiation intensity comparisons are made with recently conducted tests in the Electric Arc Shock Tube (EAST) facility at NASA Ames Research Center. The spectral range spanned from vacuum ultraviolet wavelength of 115 nm to infrared wavelength of 1400 nm. The analysis is done for 9.5-10.5 km/s shock passing through room temperature synthetic air at 0.2, 0.3 and 0.7 Torr. The comparisons between model and measurements show discrepancies in the level of background continuum radiation and intensities of atomic lines. Impurities in the EAST facility in the form of carbon bearing species are also modeled to estimate the level of contaminants and their impact on the comparisons. The discrepancies, although large in some cases, exhibit order and consistency. A set of tests and analyses improvements are proposed as forward work plan in order to confirm or reject various proposed reasons for the observed discrepancies.

I. Introduction

As part of the Vision for Space Exploration, NASA and its contractor partners are designing a lunar return capable Orion reentry capsule that will carry a 5-member crew safely back to Earth. The thermal protection system (TPS) for the 5.0 m diameter Orion capsule is being designed for an 11 km/s entry velocity skip trajectory with a 2500 nmi downrange. Radiation from the high temperature shock layer formed in front of the 5.0 m diameter vehicle at such high speed will be a significant source of vehicle heating. The CEV Aeroscience Project (CAP) is responsible for defining the aerodynamic and aerothermal environments, including radiative heating for all re-entry trajectories. Radiative heating, while not a large component of the integrated heat load, is almost as high as the convective component for some time in the entry trajectory. Radiative heating predictions and associated uncertainties are therefore critical in TPS material testing, qualification, and risk assessment.

Since flight tests measuring shock layer radiation are expensive and rare, engineers have to rely on physics based models with a dose of empiricism via anchoring to reliable ground test data. Radiative heating is predicted using codes like NEQAIR, HARA, etc. These are essentially computational models that compute radiative intensity from electronic transitions in atoms and molecules, including bound-free transitions and free electron radiation. The work presented in this paper summarizes the comparisons between the current state-of-the-art models against the

¹ Aerospace Engineer, Reacting Flow Environments Branch, Deepak.Bose@nasa.gov

² Graduate Research Assistant, Department of Mechanical and Aerospace Engineering

³ Senior Research Scientist

only source of ground test data; the NASA Ames Electric Arc Shock Tube (EAST) facility. The details of the facility can be found elsewhere and will only be discussed briefly. The purpose of this work is to evaluate the predictive capability of our state-of-the-art radiation models, investigate the causes for disagreement, and provide a strategy to bridge the gap between model predictions and test data. With these objectives in mind, a comprehensive shock tube test program was designed to cover the entire radiation spectrum relevant for Earth entry radiation. Spectrally and spatially resolved radiation intensities were measured using calibrated spectrographs. Past efforts that compared nonequilibrium and equilibrium radiation measured in the Phase I EAST testing to the results of HARA and NEQAIR can be found in Refs. RRR. Phase I testing covered only a small portion of the data necessary to validate radiation model. This paper deals with more recent Phase II data which obtained is the most comprehensive and detailed air shock layer radiation data obtained to date.

The focus of this paper is on identifying the discrepancies between the shock tube data and model predictions, listing the possible causes for the discrepancies based on observations, and planning future tests to confirm or reject hypotheses.

II. CEV Shock Layer Radiation

In the current design cycle, the CEV TPS is being designed for what is known as the Entry Interface 2 (EI2) skip trajectory with 2500 nmi down range. Emergency trajectories, that dive deeper into the atmosphere at high speed, typically subject the vehicle to more severe aerodynamic (pressure, shear, etc.) and aerothermal environments (convective and radiative), are also considered, but only from a material survivability perspective. Due to a smaller integrated heat load the emergency trajectories are not used to design the TPS thickness.

Figure 1 shows the freestream pressure and vehicle speed for EI2 skip and emergency trajectories, two key flow parameters that determine radiative heating. The curves in Fig. 1 show only a limited portion of the trajectory where radiation is deemed important. The fully margined radiative heating at the stagnation point is shown as varying color of the curves. At peak heating, the radiative component is as high as the convective heating. It is also important to mention that the shock stand-off distance, which determines the thickness of the radiating layer, is about 25-30 cm. The nonequilibrium relaxation zone predicted based on the state-of-the-art relaxation and kinetics rates is only about 2-3 cm.^{RRR} It is therefore predicted that radiative heating for CEV will be dominated by a shock layer in thermal and chemical equilibrium. The length (thickness) of the nonequilibrium zone, of course, has to be confirmed from the EAST data. Near the peak heating point the shock layer is at 10,000-11,000 K and is fully dissociated into atoms with an ionization fraction of about ~1-7%. In this paper we will focus on radiative heating at these conditions in thermochemical equilibrium. Reference () discusses the state of the CEV shock layer as predicted by the state-of-the-art CFD code, DPLR.

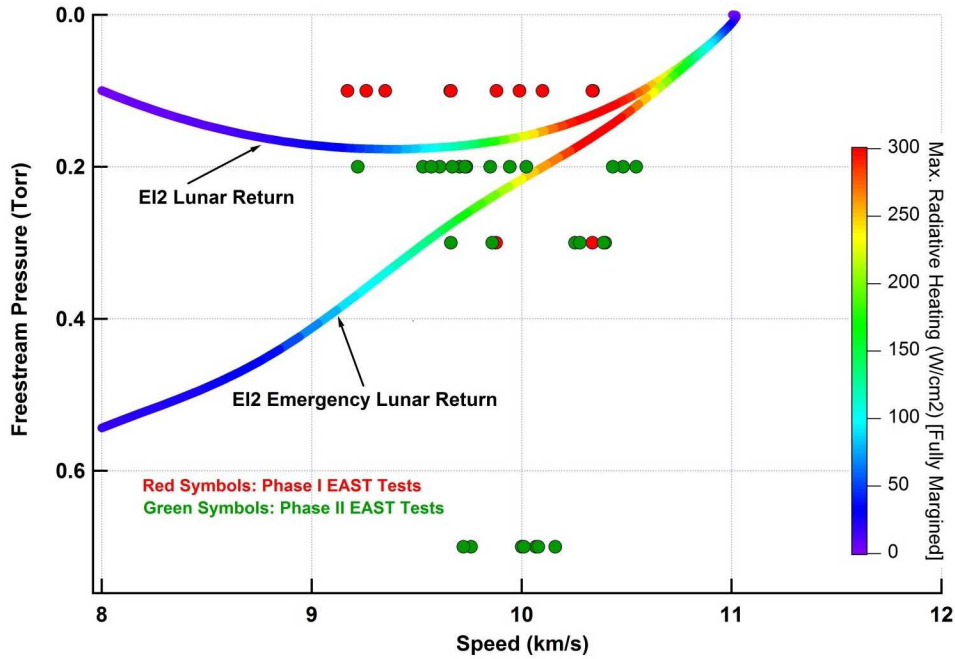


Figure 1. A portion of Entry Interface 2 (EI2) skip and emergency lunar return trajectories for CEV. The symbols represent Phase I and II EAST testing conditions. The color of the lines show maximum radiative heating with a 45% margin used for design.

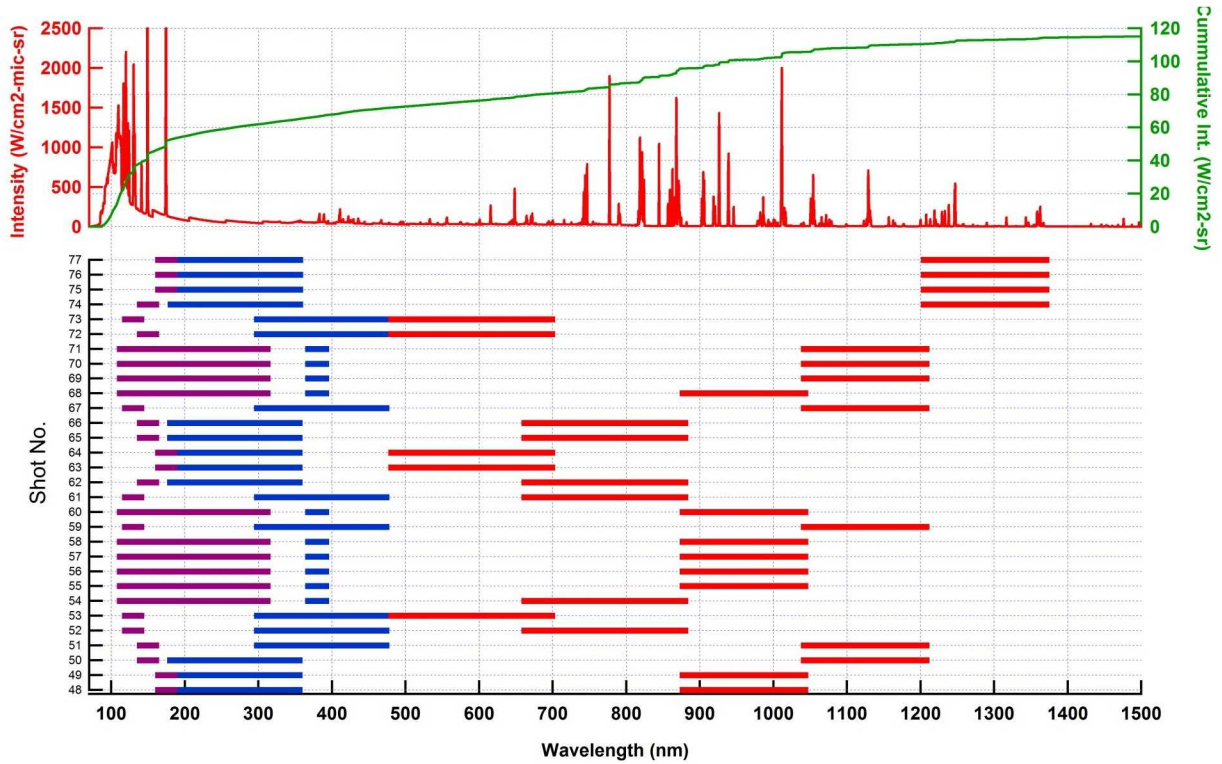


Figure 2. A sample of simulated CEV stagnation point radiation spectrum and spectral coverage in different EAST shots. The color of the bars represent different cameras. Red

camera covers visible and infrared regions. Blue camera covers the ultraviolet regions. VUV camera coverage is represented by purple bars.

III. Test Program

The Electric-Arc Shock Tube (EAST) facility at NASA Ames Research Center was recently used to measure shock induced radiation at conditions relevant for CEV lunar return (9.5-11 km/s). A suite of instruments were employed to measure intensity of post shock radiation, chief among them are the calibrated spectrographs that measured spatial and spectral scans of shock layer intensity. The test infrastructure and instrumentation details are presented in Ref. 2. For Phase I testing that included shots at 0.1, 0.3, and 1.0 Torr, the data comparisons with model were presented in Refs. 3 and 4. Unfortunately, 0.1 Torr tests yielded only a few shots with reasonable test times.

Past validation of air radiation model has indentified some issues such as presence of excessive continuum radiation in the UV that was not predicted by NEQAIR.^{RRR} Although, there were only limited number of comparisons made, it was also found that NEQAIR under predicted radiative intensities, by a large amount in some cases.^{RRR}

Since the last test series (Phase I), much new data has been obtained at 0.2, 0.3, and 0.7 Torr and shock speeds of 9.5-11 km/s. The Phase II test series, which is shown in Fig. 2, has more than doubled the available test data and explored a more relevant parameter space (see Fig. 1). Unlike Phase I testing where we had only a limited number of low pressure shots (< 0.3 Torr) that produced thermochemical equilibrium, Phase II testing has produced a large volume of spectral data with such shots. These tests also provided many repeated shots as seen in Fig. 2. The new data gives us the best opportunity we have ever had in validating and assessing the predictive capability of NEQAIR for high speed Earth entries. This test series also provides the first ever opportunity to perform some validation of the important VUV portion of the spectrum. Due to strong absorption of the VUV, it has the potential to play a key role in the boundary layer heat transfer in flight. Past studies have shown the VUV radiation will very likely be strongly absorbed in the boundary layer and re-appear as convective heating.^{RRR}

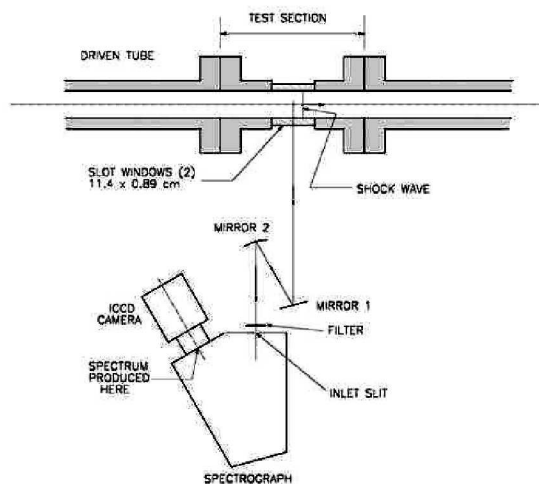


Figure 3. A schematic of the EAST test section and imaging spectrograph

IV. NEQAIR Model

The modeling of shock layer radiation at NASA Ames Research Center is done using a line-by-line radiation program known as Nonequilibrium Air Radiation (NEQAIR) code. RRR NEQAIR computes spontaneous emission, absorption, and stimulated emission due to transitions between various energy states of chemical species present along a line-of-sight. Individual electronic transitions are considered for atoms and molecules. The molecular band systems are resolved for each rotational line. Bound-free and free-free radiation are also considered as outlined in Ref. 19. The distribution of electronic state population is determined by quasi-steady state model of Park,⁷ which solves a set of master equations comprising of electron impact excitation, de-excitation, ionization, recombination, and radiative depopulation. The term in the master equation due to radiative absorption is taken into account using a crude approximation of an escape factor. However, due to high pressure environment in the shock layer, the radiative population and depopulations terms are, in general, small compared to electron impact collision term.

In this work since we are only concerned with thermochemical equilibrium radiation, we generate radiation spectrum from the shock tube using a line of sight that runs perpendicular to the tube axis assuming a constant property gas with a length equal to the diameter of the tube. The constant properties of the shocked gas is obtained from CEA. RRR The effect of boundary layer in the tube wall is ignored. This is likely to be important only in the analysis of high pressure data where boundary layer absorption is significant or in the case of VUV radiation where boundary layer absorption may be important at all pressures analyzed here. The reduction of the effective tube cross section below the diameter of the tube due to boundary layer growth is another factor that is ignored here. In any case all factors introduce error in one direction. In other words, all these assumptions will tend to increase the model predictions compared to the measured data. Therefore predicting higher radiation than what is measured does not necessarily make the model conservative, but predicting lower radiation intensity is definitively a cause for concern and must be margined against for flight design.

V. Comparisons of Model Predictions with Measurements

Due to a large volume of data obtained it is not possible to present comparison with full dataset in this publication. In this paper, we will present a representative sample of comparisons. We will, however, emphasize the 0.2 and 0.3 Torr cases that are more relevant for CEV flight [see Fig. 1] and present 0.7 Torr cases when necessary.

Data will be presented in the format shown in Fig. 4. The top left panel shows the absolute intensity ($W/cm^2-\mu\text{-sr}$) as measured by the spectrograph using a color map over wavelength and distance in the flow direction. The top-right panel shows the integrated intensity over wavelength (the limits are defined by the vertical dashed lines) in the units of $W/cm^2\text{-sr}$. This panel shows the nonequilibrium overshoot, if present, and subsequent relaxation to thermochemical equilibrium characterized by steady state intensity. In the ultraviolet portions of the spectrum, arrival of the driver gas in the form of metal vapor lines can often be seen. The arrival of the driver gas represents the end of useful test time. The bottom-left panel shows several curves as defined below.

- The solid red curve shows the measured spectrum, averaged over a finite distance to minimize noise. The chosen “steady-state” region is represented by two horizontal dashed lines. The attempt here is to pick a steady state region before the end of the test time. When a steady-state is not reached, we choose something toward the end of test time assuming it provides a lower bound of what would have been the steady state radiation.

- The solid blue curve shows NEQAIR simulated spectrum assuming thermochemical equilibrium of shocked air obtained using CEA.RRR No impurities are added in default simulations.
- The dashed red curve shows a running integrated intensity (integrated over wavelength) in W/cm²-sr from left to right of the measured spectrum.
- The dashed blue curve represents a running integrated intensity in W/cm²-sr from left to right of the NEQAIR spectrum.
- In some cases a solid green curve will be shown. This curve is intended to apply modifications to the default simulation. The modifications include addition of impurities and elevation of the spectrum by a constant intensity to get a better match with data. These curves will be discussed on a cases-by-case basis in the discussion.

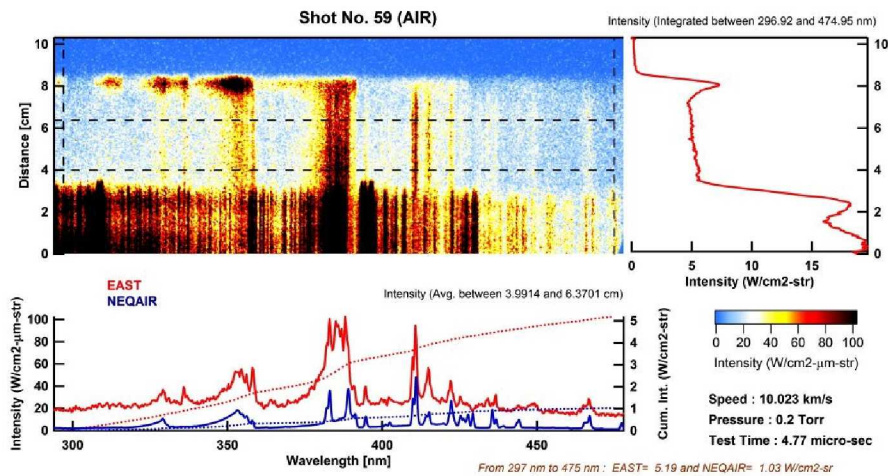


Figure 4. A sample EAST measurement and NEQAIR simulation comparison.

The dataset is organized into wavelength regions covered by the spectrograph. The regions are shown as red, blue and purple bars in Fig. 2. We begin with the “Red” camera regions shown as red bars in Fig. 2 covering the visible and IR spectrum. We then cover the “Blue” camera regions shown as blue bars in Fig. 2 covering mostly UV regions and portions of visible spectrum. Finally, we cover the VUV camera regions shown as purple bars in Fig. 2 covering the VUV wavelengths with some coverage of UV spectrum as well.

“Red” Camera

R-1 (476-704 nm)

In this spectral range several atomic lines intensities are apparent as can be seen in Fig. 5. Shot 64 at 0.3 Torr appears to reach near equilibrium steady state. Shot 72 at 0.2 Torr, however, falls short of equilibrium in the 7.7 μ s of test time. For the sake of comparisons, it is assumed that the intensities at the chosen location of comparison provide a lower bound of the true equilibrium radiation. In both cases, although NEQAIR predicts all N and O lines, the overall integrated radiation is predicted to be much lower than what is observed in measurements. A major component of the radiation appears to be the background radiation, which raises the floor of the measured spectrum. The cause of the background radiation is presently unknown. It must be noted that NEQAIR includes possible continuum radiation from bound-free and free-free transitions. The bound-bound line intensities in NEQAIR predictions appear to agree well with measurements.

Another noteworthy feature in this wavelength region is an intensity spike that appears immediately behind the shock. The spike is repeatable and consistently seen in all shots with varying magnitude. It is observed that the relative height of the spike (relative to equilibrium intensity) decreases as the shock speed and pressure increase pointing to nonequilibrium overshoot phenomena. In this paper we will however not focus on nonequilibrium phenomena other than making some passing references.

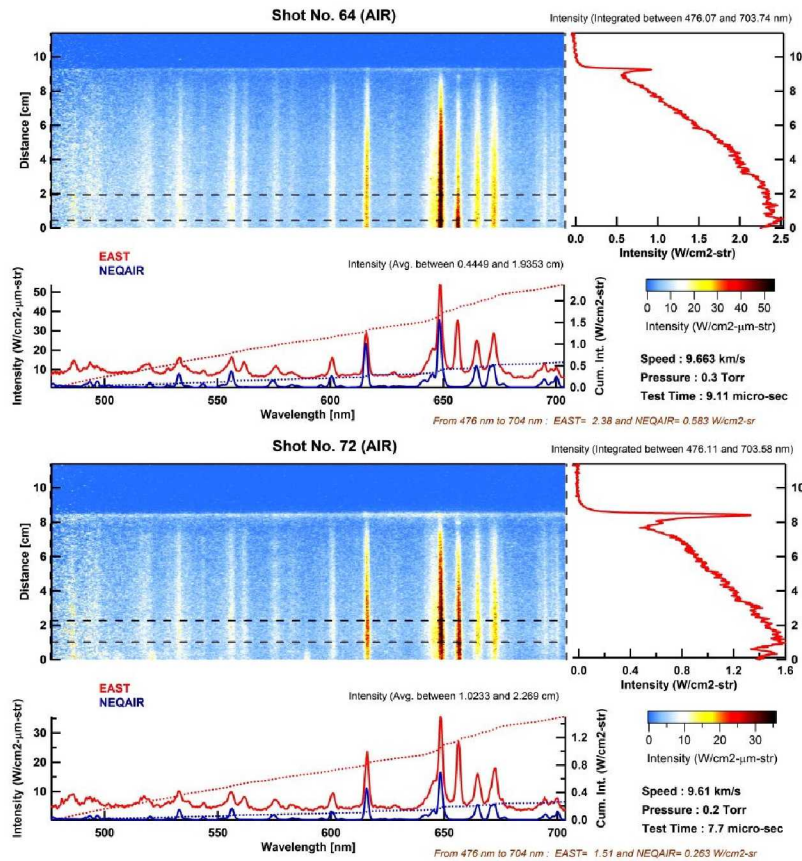


Figure 5: Sample comparisons of NEQAIR predictions and EAST measurements in 476-704 nm range. (a) 9.663 km/s, 0.3 Torr and (b) 9.61 km/s, 0.2 Torr

R-2 (658-885 nm)

This wavelength region has some intense atomic N and O lines as shown in Fig. 6. Although Shot 66 seems to have reached steady state equilibrium, in Shot 62 the choice of equilibrium may be questionable. The NEQAIR comparisons of integrated intensities, however, are excellent in the wavelength range for both shots. The line intensities in general are overpredicted, while the background continuum is not predicted, which fortuitously leads to a good overall agreement. The nonequilibrium intensity spike also exists in the wavelength range at 0.2 Torr, but not at 0.3 Torr or at higher pressure shots that are not presented. As stated earlier, the relative height of the nonequilibrium spike diminishes with shock speed at a given pressure. In summary, the line

intensities are overpredicted by NEQAIR, but the background continuum that is seen in the measurement is not.

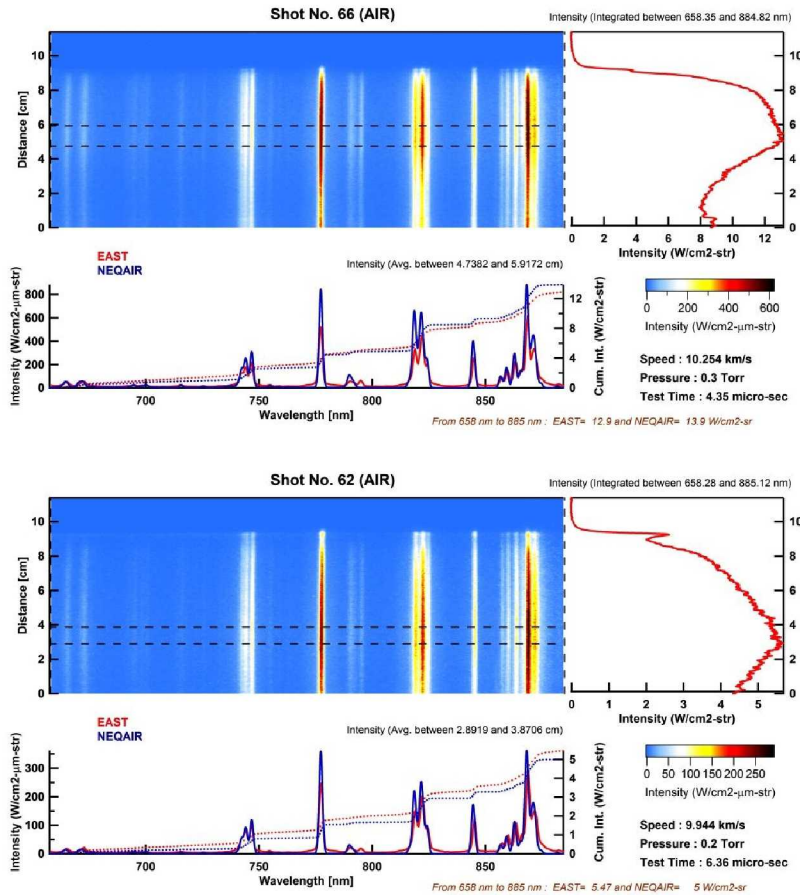


Figure 6: Sample comparisons of NEQAIR predictions and EAST measurements in 658-885 nm range. (a) 10.254 km/s, 0.3 Torr and (b) 9.944 km/s, 0.2 Torr

R-3 (875-1050 nm)

Like the previous region, this wavelength region is dominated by strong atomic N and O lines as shown in Fig. 7. In this region, NEQAIR line intensities are much stronger than what is measured in EAST. It is important to point out that the areas under line intensities should be compared rather than peak intensities. At first, it may appear that boundary layer absorption, which is not included in the NEQAIR calculations, may be the reason for overprediction of line intensities. However, at 0.7 Torr shown in Fig. 7(a), where boundary layer absorption is expected to be more, the predictions of line intensities are better than at lower pressure [Figs.7 (b) and (c)].

It also appears that NEQAIR tends to overpredict line intensities as the shock speed increases. In other words, NEQAIR predictions rise faster shock speed than what the measurements show. At high speeds, the impact of radiative cooling is more prominent, which may explain reduced measured intensities. In future tests, we plan to measure electron density in the equilibrium region of the shocked gas via line broadening measurements to validate existence of correct

thermochemical equilibrium conditions. Also, NEQAIR analysis will estimate the effect of radiative cooling.

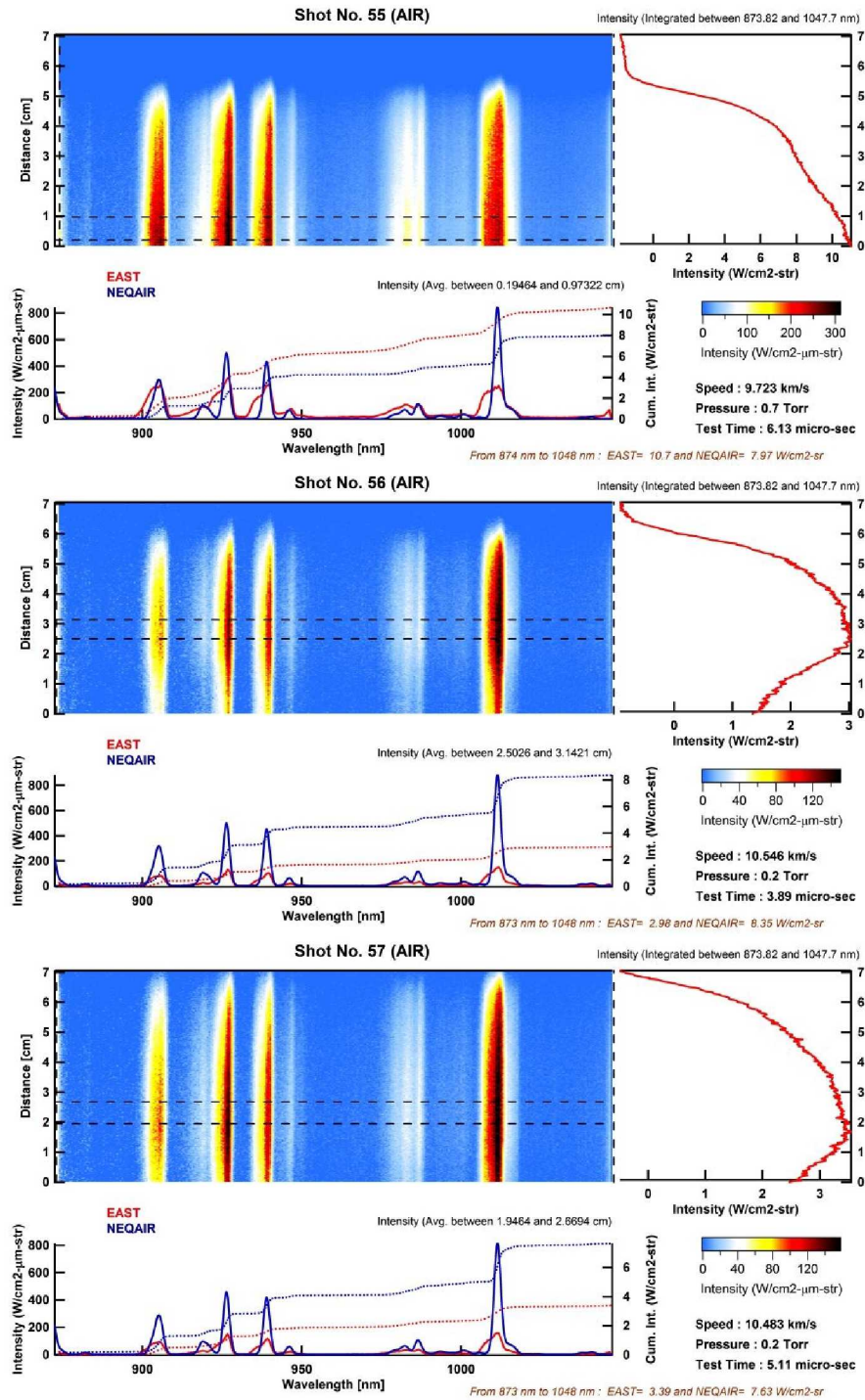


Figure 7: Sample comparisons of NEQAIR predictions and EAST measurements in 873-1048 nm range. (a) 9.723 km/s, 0.7 Torr, (b) 10.546 km/s, 0.2 Torr, and (c) 10.483 km/s, 0.2 Torr

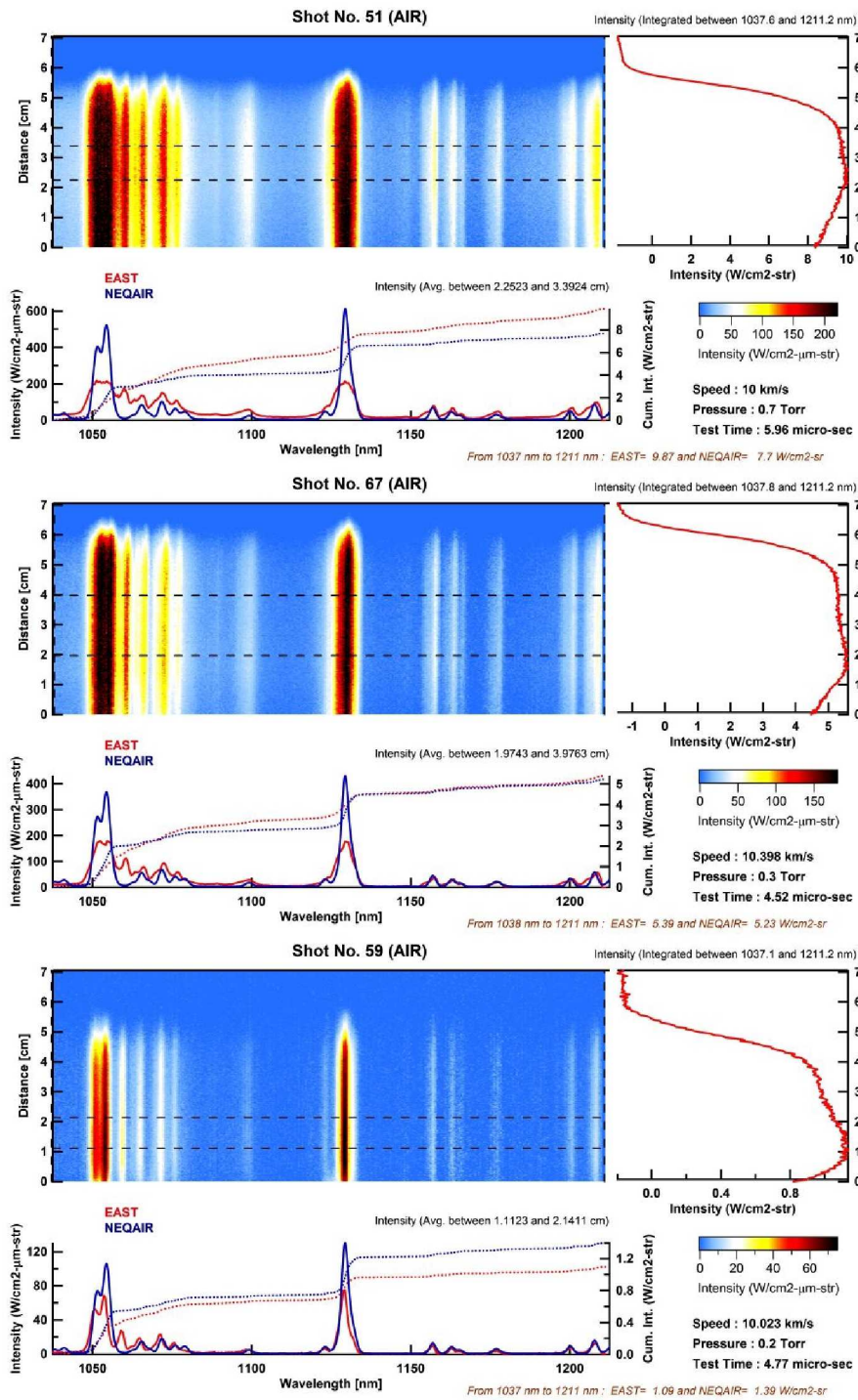


Figure 8: Sample comparisons of NEQAIR predictions and EAST measurements in 1038-1211 nm range. (a) 10 km/s, 0.7 Torr, (b) 10.398 km/s, 0.3 Torr, and (c) 10.023 km/s, 0.2 Torr.

R-4 (1040-1210 nm)

This is another region with strong atomic line radiation as seen in Fig. 8. NEQAIR seems to agree well the integrated intensity. The shocked gas shows a cleaner equilibrium compared to what was observed in other regions. Upon closer look, the integrated line intensities are actually somewhat overpredicted by NEQAIR. At 0.3 Torr and 10.398 km/s, the integrated intensities agree very well. Like the last spectral range, this agreement is due to fact that line intensities are overpredicted but the background continuum, that is only seen in measurements, makes up the difference. In addition there is an unpredicted feature at 1060 nm. At 0.7 Torr and 10 km/s, NEQAIR underpredicts line intensities, as well as the integrated intensity. This underprediction occurs despite the possibility that at high pressures, there is an increased likelihood of boundary layer absorption in the shock tube, which is not modeled. It must also be mentioned that at 0.7 Torr the shock speed is lower than that in 0.3 Torr (10.0 km/s vs. 10.398 km/s), which is another reason for the difference in the agreements. It is generally noticed, that NEQAIR simulations are more sensitive to changes in speed than what is seen in measurements. At 0.2 Torr, where background intensity is relatively small, the NEQAIR integrated intensity ends up higher than what is measured. In summary, all three pressure show over prediction of line intensities by NEQAIR.

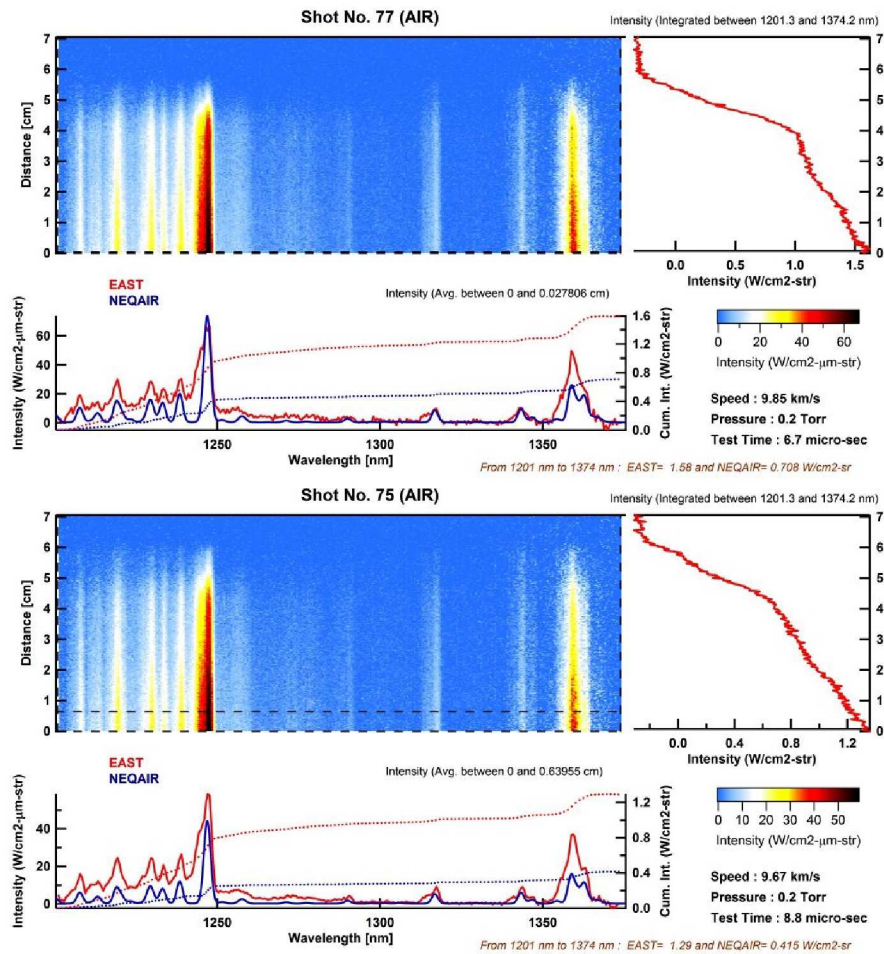


Figure 9: Sample comparisons of NEQAIR predictions and EAST measurements in 1200-1374 nm range. (a) 9.85 km/s, 0.2 Torr, (b) 9.67 km/s, 0.2 Torr

R-5 (1200-1375 nm)

This region is the longest wavelength region where data were taken. The atomic line intensities are not very strong and the background continuum, especially between 1200-1250 nm adds significant radiation, as seen in Fig. 9. As in other regions, background radiation of this level is not seen in NEQAIR predictions. It should also be noted that the shocked gas has probably not reached equilibrium in either of the shots shown. However, they do provide a lower limit to what would be the equilibrium radiation and NEQAIR underpredicts that. A kinked profile is seen in the intensity profiles with distance. The reason for the kink is not known. It could be a secondary compression wave, which increases the intensity further. Since it is not clear whether the shock has reached equilibrium we assume this comparison to be inconclusive until further testing

Blue Camera

In the UV region, the arrival of driver gas contamination can be clearly seen as metal vapor lines of aluminum and tungsten fill the spectrum. The nonequilibrium intensity overshoot of radiation is also seen in lower speed and lower pressure shots. The UV region is also dominated by molecular systems such as CN violet and N₂⁺⁽¹⁻⁾. In addition atomic lines of N and C can be seen. CN and C lines appear due to carbon-based impurities in the shock tube.

B-1 (300-475 nm)

This portion of the spectrum is dominated by atomic N, CN violet, and N₂⁺⁽¹⁻⁾ radiation. These features are identified in Fig. 10. In the lower speed shot (9.61 km/s) molecular band radiation is more prominent, while higher speed (10.398 km/s) shot has stronger N atomic lines. The default NEQAIR runs that are presented thus far are done with a pure mixture of N₂ and O₂ without any carbon bearing species. In order to estimate the level of impurities we add atomic carbon in pure air to find a best match with the observed signal of CN violet. The equilibrated shocked air with carbon impurity forms C₂, C, and CO, in addition to CN. In Figs. 10 (a) and (b), the spectrum shown in green contains the effect of carbon bearing impurities and an additional increase in baseline radiation to better match the data. As seen in the figures, carbon impurities alone cannot explain the discrepancy.

In Fig. 10 (a), the modified NEQAIR spectrum (shown in green) was created by adding 12% carbon by mole to undissociated air. The contribution of CN violet is not very significant in this shot due to its high speed (10.398 km/s). As a result, addition of carbon only makes a small change in the spectral features. The spectrum was also elevated by 60 W/cm²-μ-sr to account for the lack of background continuum in NEQAIR simulations. It is observed that atomic lines predicted by NEQAIR are not as strong as the ones measured if the green and the red spectra are compared in Fig. 10 (a).

In Fig. 10 (b), CN violet contribution is larger due to a lower shock speed resulting in a lower level of molecular dissociation. In this shot, a good match is found by adding 8% carbon by mole to undissociated air and elevating the spectrum by 10 W/cm²-μ-sr. The rotational temperature, which determines the decay rate of the intensity of CN violet ($\Delta v=0$) manifold, between 385-365 nm, is also predicted well.

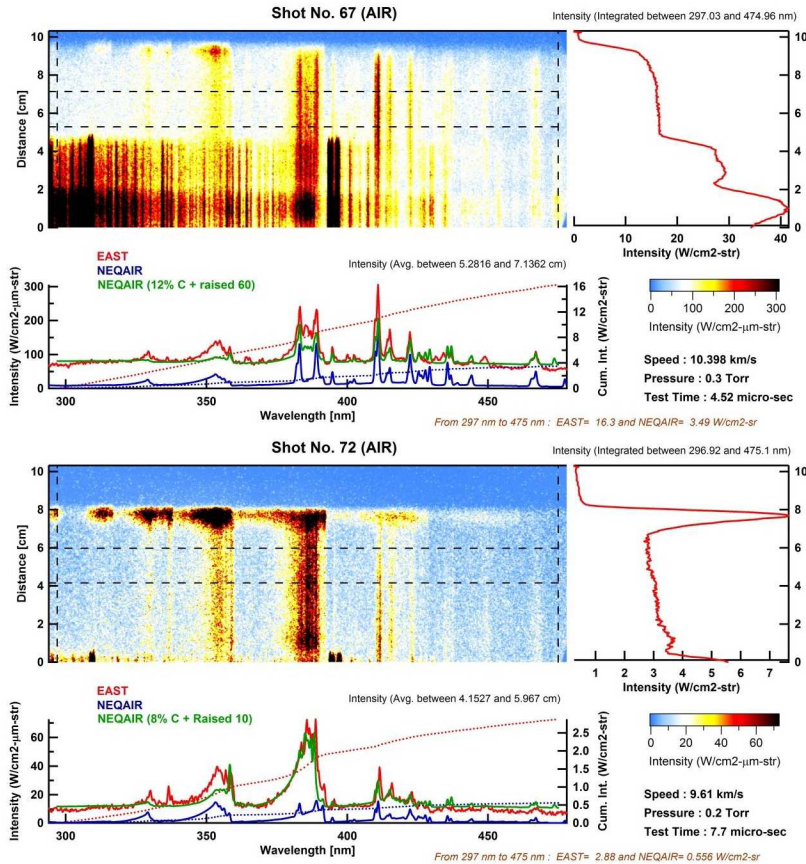


Figure 10: Sample comparisons of NEQAIR predictions and EAST measurements in 297-475 nm range. (a) 10.398 km/s, 0.3 Torr, (b) 9.61 km/s, 0.2 Torr

B-2 (363-397 nm)

This region shows the $\Delta v=0$ vibrational manifold of CN violet and N₂⁺⁽¹⁻⁾ systems shown in Fig. 11. A couple of prominent N lines are also seen. Again, the baseline predicted by NEQAIR is much lower than what is measured. Obviously, CN violet is missing from these calculations as no impurities were added. The equilibrium steady state is reached in both shots shown in Fig. 11. The nonequilibrium overshoot appears in Fig. 11 (b) (9.73 km/s, 0.2 Torr), and not in Fig. 10 (a) (10.39 km/s, 0.3 Torr), because of lower speed and lower pressure. Addition of carbon impurities shows that the measured spectrum can be matched very well by adding 12% carbon to undissociated air and raising the baseline by 15 W/cm²-μ-sr. The rotational temperature, which is a measure of the intensity decay rate between, say, the peak at 385 nm to 365 nm, is also predicted well by pure thermochemical equilibrium.

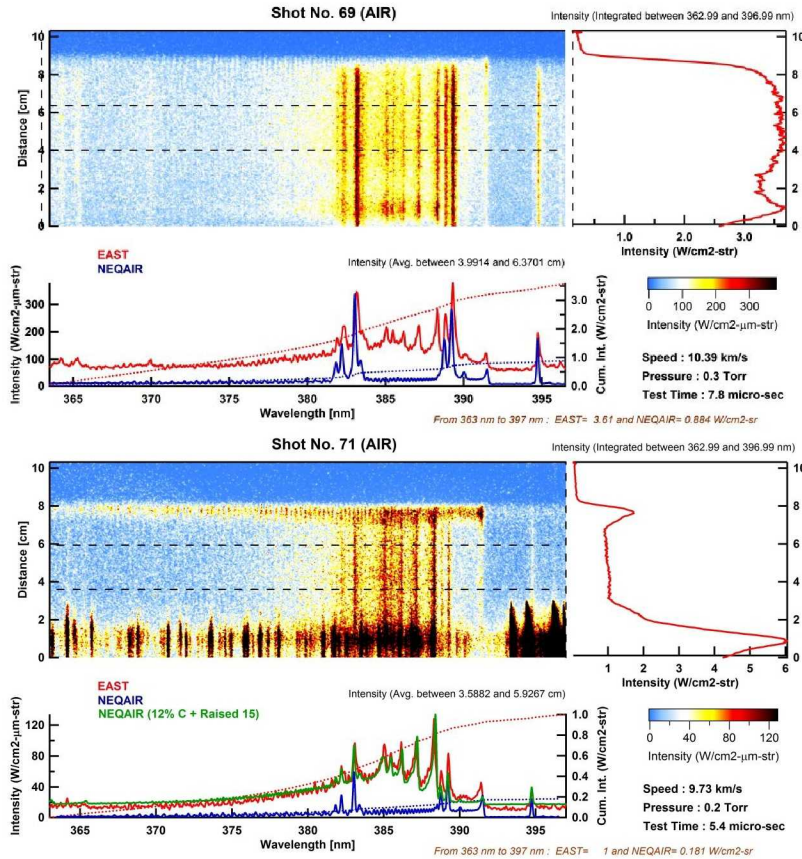


Figure 11: Sample comparisons of NEQAIR predictions and EAST measurements in 363-397 nm range. (a) 10.39 km/s, 0.3 Torr, (b) 9.73 km/s, 0.2 Torr

B-3 (225-360 nm)

This is a quiet UV wavelength region shown in Fig. 12. The features visible are the $\Delta v=2$ manifolds of N₂⁺⁽¹⁻⁾ and CN violet systems. In addition, C 248 nm line is also visible. The contribution of background continuum is significant compared to line intensities and is not predicted by NEQAIR, which falls far short of what is measured. The strong intensity found in the measured spectra between 200-240 nm is not seen in NEQAIR simulations. This feature may not be real as the camera sensitivity drops off at this wavelength range. We will revisit this region later when we discuss VUV measurements.

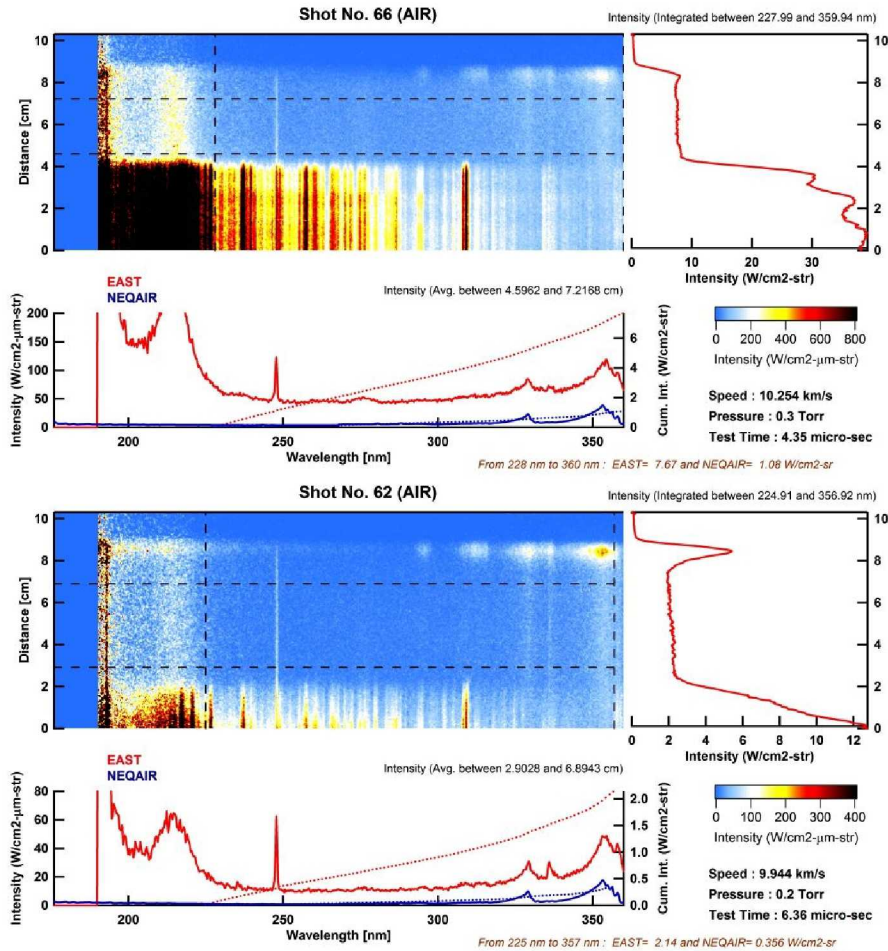


Figure 12: Sample comparisons of NEQAIR predictions and EAST measurements in 363-397 nm range. (a) 10.39 km/s, 0.3 Torr, (b) 9.73 km/s, 0.2 Torr

Vacuum Ultraviolet Camera

The VUV data were measured using a vacuum optical system and a lithium fluoride window in the test section to avoid transmission losses in outside air and due to window cut-off. The details of the setup and measurements can be found in Ref RRR. Despite best efforts, the optical path in the spectrograph is affected by air leaks into the spectrograph, which made the data in some portions of the spectra either unusable or in some cases useable only qualitatively. Since VUV absorption in air is due to oxygen, our future plan includes using a nitrogen purge in the optical system to keep the oxygen concentration very low. Although not perfect, the current set of measurements gives us the first comprehensive look at the mysterious VUV radiation in a shock layer. This portion of the radiation is responsible for about 40% of the overall incident radiation on the vehicle boundary layer edge.

In these measurements magnitude of VUV radiation suffers from absorption via two mechanisms. First, the absorption of the radiation outside the shock tube in the optical path as mentioned before. Second, in the shock tube boundary layer, that is colder and possibly more contaminated than the core flow. The measurement, however, should give us a lower bound of the actual VUV radiation. As it turns out NEQAIR often underpredicts the VUV data pointing to a need for a radiative heating margin in the CEV TPS design.

VUV-1 (160-190 nm)

This VUV region shows one N doublet at 174 nm and a C line at 166 nm shown in Fig. 13. The integrated intensity of N lines is significantly underpredicted, by about a factor of 2. This is despite possible absorption in the shock tube boundary layer. Upon closer look, it also appears that broadening of N lines (at 174 nm) measured is larger than the width of NEQAIR lines scanned with instrument function. It is confirmed that the measured line width is not limited by instrument resolution, by examining the test at 0.7 Torr which shows increased broadening using the same instrument. A smaller line broadening in simulation would result in more self-absorption inside the tube resulting in lower intensity. We plan to perform high resolution measurements in VUV to update and validate NEQAIR line broadening data in future test series.

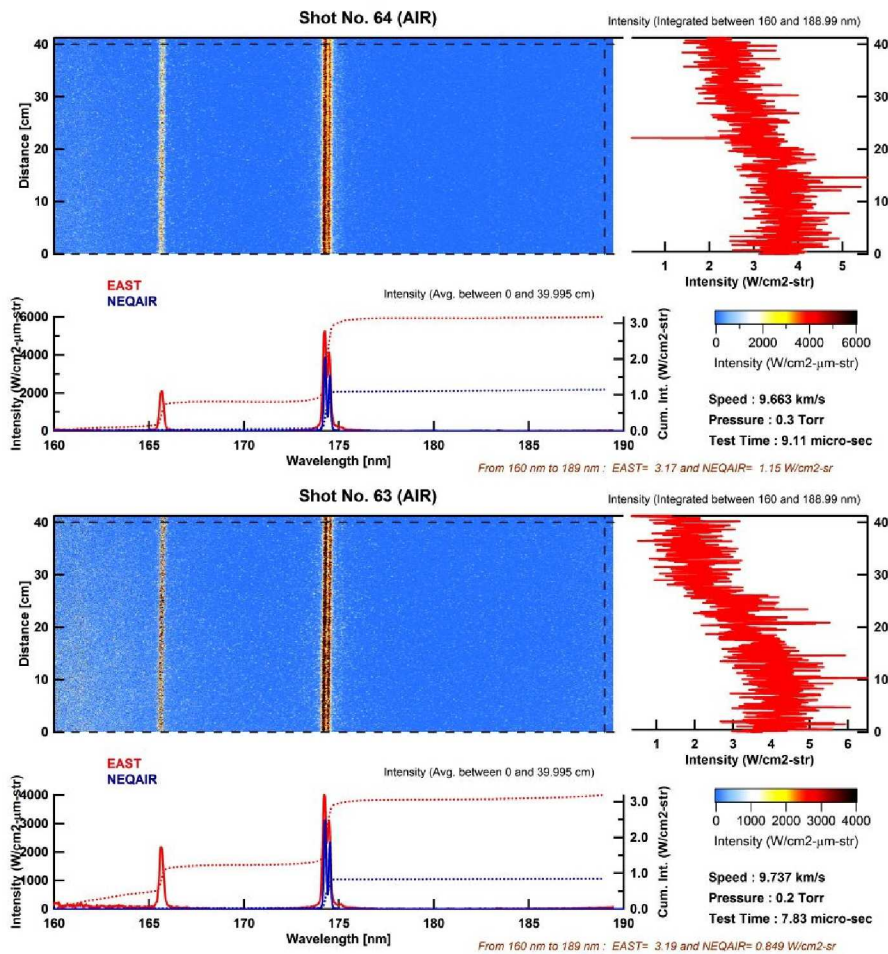


Figure 13: Sample comparisons of NEQAIR predictions and EAST measurements in 160-189 nm range. Spatial resolution is not available for these measurements. (a) 9.663 km/s, 0.3 Torr, (b) 9.737 km/s, 0.2 Torr

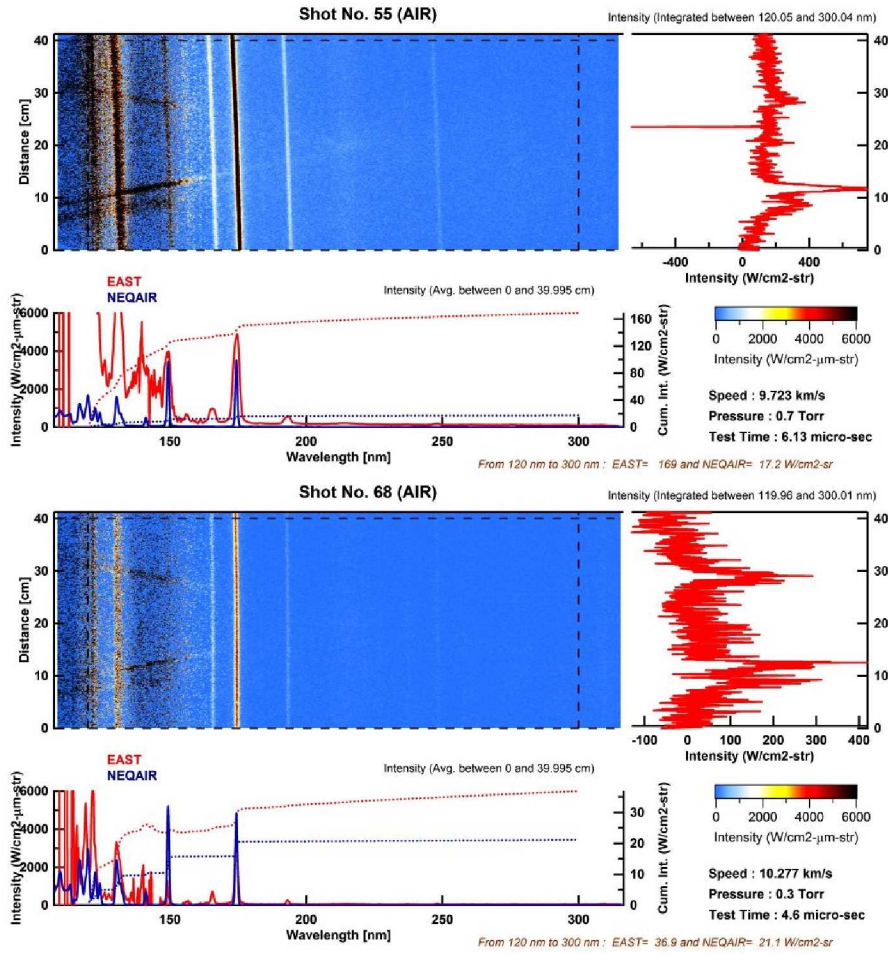
VUV-2 (115-144 nm)

Radiation in portions of this wavelength region suffers significantly from absorption due to molecular oxygen (due to air leaks) in the optical path outside the shock tube. Based on the absorption properties of molecular oxygen, the data in this range is useful only between, say 126-

Figure 14: Sample comparisons of NEQAIR predictions and EAST measurements in 115-145 nm range. Spatial resolution is not available for these measurements. (a) 10.011 km/s, 0.7 Torr, (b) 10.398 km/s, 0.3 Torr, and (c) 10.023 km/s, 0.2 Torr

VUV-3 (120-300 nm)

This region shown in Fig. 15 covers a wide wavelength range that extends into the UV. Only a couple of N lines can be seen (150 and 174 nm) as the data becomes noisy due to oxygen absorption outside the shock tube. In these shots, N 174 nm is predicted in terms of integrated area at 0.2 and 0.3 Torr shots, but again, is significantly underpredicted at 0.7 Torr. Again, a larger pressure broadening is evident in measurements at 0.7 Torr. The atomic line at 150 is significantly over predicted by NEQAIR, but it is difficult to make a firm conclusion due to noise in measurements.



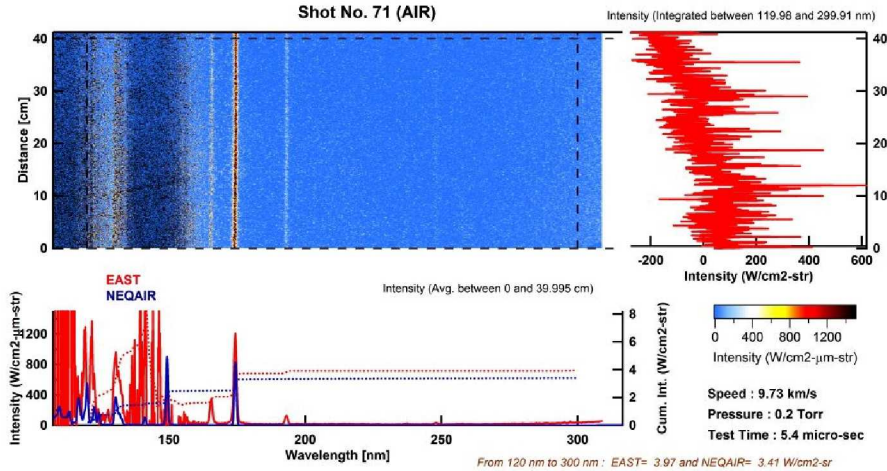


Figure 15: Sample comparisons of NEQAIR predictions and EAST measurements in 120-300 nm range. Spatial resolution is not available for these measurements. (a) 9.723 km/s, 0.7 Torr, (b) 10.277 km/s, 0.3 Torr, and (c) 9.73 km/s, 0.2 Torr

VI. Discussion

Summary of Observations:

The observations made in the last section can be summarized as follows. One of the main findings is the presence of background radiation throughout the entire spectral range. Despite modeling bound-free and free-free radiation, NEQAIR is unable to predict the magnitude of the background continuum. Second, there is a consistent underprediction of atomic line intensities in the VUV and UV regions. The underprediction gradually turns to good prediction in the visible part of the spectrum, which is followed overprediction of atomic lines in the IR regions. It is also noticed that NEQAIR predicted intensities are more sensitive to changes in shock speed than what is seen in measurements. Given these structural discrepancies, it is difficult to apply the present model to flight conditions for TPS design without significant margins.

Root Cause Analysis:

Based on the observations, in this section we present a list of hypotheses that may explain the discrepancies. It must be pointed out that the reason for the discrepancy may be lie in modeling deficiencies or in inadequacies and uncertainties in EAST facility or measurement set up. The hypotheses are listed in Fig. 16, and are matched with the observations that they help explain. A green circle indicates that the given hypothesis explains the chosen observation. A red circles shows that the hypothesis will not explain the observation, and an orange circle indicates a partial explanation.

1. “Additional molecular systems needed”: It is possible that additional molecular systems such as CO, NO, and lower hydrocarbons (from contaminants) may exist in the boundary layer, which is at a lower temperature than the core flow. These molecules may radiate as bands with low intensities compared to atomic line

- radiation originating in the core flow. These molecular bands may cover a large portion of the spectrum and may appear as “background continuum”.
2. “Baselining Error”: It is possible that a proper baseline was not chosen when raw counts were converted into absolute intensity. The current process subtracts dark noise from the raw measurements to baseline the spectrum. The process will be reviewed further for possible reasons that may explain the appearance of “background continuum”.
 3. “Thermochemical equilibrium not achieved”: In NEQAIR simulations, we assume a thermochemical equilibrium condition for the shocked gas using CEA. It is possible due to a variety of reasons that in the EAST we did not achieve proper thermochemical equilibrium.
 4. “Radiative and Sidewall Cooling”: It is assumed that the total enthalpy of the flow does not change as the gas passes through the shock and achieves equilibrium. Loss mechanisms such as boundary layer interaction with cold tube walls and radiative cooling could reduce the enthalpy, and thereby, prevent the gas from achieving correct equilibrium.
 5. “NEQAIR line broadening data inadequate”: The self-absorption of radiation in the shock tube is dependent on broadening of atomic lines. Under the conditions investigated here, Stark and Doppler broadening are dominant. From the VUV spectra, especially at 0.7 Torr, it appears that NEQAIR line broadening is smaller than what is measured. This would explain a consistent underprediction of VUV radiation by NEQAIR. The current dataset for Stark broadening is taken from Greim, but the broadening parameters are extrapolated to different electron densities and temperatures using empirical expression that needs validation.
 6. “Contamination is shock tube”: The flow in EAST is undoubtedly contaminated as evidenced by the appearance of C, CN, H lines in pure synthetic air consisting of only oxygen and nitrogen. The contaminants are known to exist in vapor phase, but may also exist in the form of particles (soot), which may radiate as a black body. It is hypothesized that particles may be swept up from the tube walls as the shock passes through.
 7. “High lying transitions”: NEQAIR currently does not include many bound-bound transitions between atomic states with principal quantum number of 4 or more. These high lying transitions are expected to be broad and numerous due a large number of such states. Together they could explain a portion of the “background continuum”, although mostly in the visible and the IR regions.

Key Observations	Root Causes for disagreement						
	Additional molecular systems needed	Baselining error	Thermochemical equilibrium not achieved	Radiative or sidewall cooling	NEQAIR Line broadening data inadequate	Contamination in shock tube	High lying transitions needed
Background Radiation not predicted	●	●	●	●	●	●	●
Underprediction of atomic lines in VUV,UV and visible	●	●	●	●	●	●	●
Overprediction of atomic lines in IR	●	●	●	●	●	●	●
Predicted intensity rises rapidly with speed	●	●	●	●	●	●	●

Figure 16. Root cause analysis based on key observations and hypotheses that may explain them.

VII. Concluding Remarks and Forward Plan

This paper presented a detailed set of spectrally resolved comparisons between NEQAIR predictions and EAST test measurements. The disagreements are large in some spectral ranges and must be margined against in flight heating predictions for TPS design. However, since there are some structural differences, it is essential that these discrepancies be resolved to attain confidence in flight predictions. We present a forward plan for testing and analysis to either confirm or reject the hypotheses presented in the last section.

Future testing plan includes the following.

1. Measure electron density to confirm existence of assumed thermochemical equilibrium conditions in the steady state region. The estimate will be based on line broadening profiles of $H\alpha$ and $H\beta$. Hydrogen will be added in trace amount.
2. Investigate to check the procedure used for baselining when raw counts are converted to absolute intensity ensuring that stray light did not reach the CCD.
3. Perform high resolution spectroscopy to measure line broadening in the VUV. Several N and O lines at 174 nm and near 130 nm are possible candidates.
4. Perform tests in another facility to get an independent validation of EAST measurements.
5. Perform a skimmer test. This test will include inserting clean and polished, one-time use metal surfaces in the test section to avoid contamination from the boundary layer

in the line of sight. The tube wall, despite cleaning, retains some contamination. Improved cleaning techniques will also be implemented.

Future enhancement plan for modeling and analysis includes the following.

1. Include tube wall boundary layer effects in the simulation using CFD. The boundary layer will possibly allow additional radiation from molecules such as NO and smaller hydrocarbons. It will also allow absorption of radiation emitted from the core flow. In addition, any possible cooling of the shocked gas due to heat transfer to the wall will be included.
2. Importance of radiative cooling in the shock tube will be estimated. This could improve predictions in high speed shots.
3. Additional molecular species that are found to exist in the tube boundary layer, including the ones from contamination, will be included in the NEQAIR simulations.
4. Bound-bound transitions among the high lying atomic states that are currently not included in NEQAIR will be included using The Opacity Project Database.

Acknowledgements

The authors would like to thank Jay Grinstead (NASA), Mark McLaughlin (NASA), Dinesh Prabhu (ELORET), Joseph Olejniczak (NASA), Chul Park (KAIST), James Arnold (UC-Santa Cruz), Aaron Brandis (University of Queensland), Christopher Johnston (NASA), and Winifred Huo (Consultant) for many useful discussions and support for this work. We would like to acknowledge the CEV Aeroscience Project (CAP) for sponsoring this work. The work of David Bogdanoff and Gary A. Allen, Jr. is performed under the NASA Contract NNA04BC25C to ELORET Corporation.

References

- ¹ Whiting, E.E., Yen, L., Arnold, J.O., and Paterson, J.A., "NEQAIR96, Nonequilibrium and Equilibrium Radiative Transport and Spectra Program: User's Manual," NASA RP-1389, Dec. 1996.
- ² Grinstead, J., Wilder, M., Olejniczak, J., Bogdanoff, D., Allen, G., and Dang, K., "Shock Heated Air Radiation Measurements at Lunar Return Conditions," AIAA-2008-1244, *Presented at the 46th AIAA Aerospace Sciences Meeting, Reno, NV, Jan 2008.*
- ³ Bose, D., McCorkle, E, Thompson, C., Bogdanoff, D., Prabhu, D., Allen, G., and Grinstead, J., "Analysis and Model Validation of Shock Layer Radiation in Air," AIAA-2008-1246, *Presented at the 46th AIAA Aerospace Sciences Meeting, Reno, NV, Jan 2008.*
- ⁴ Johnston, C.J., "A Comparison of EAST Shock Tube Measurements with a New Air Radiation Model," AIAA-2008-1245, *Presented at the 46th AIAA Aerospace Sciences Meeting, Reno, NV, Jan 2008.*
- ⁵ Park, C., "Stagnation Point Radiation for Apollo 4," *Journal of Thermophysics and Heat Transfer*, Vol. 18, No. 3, 2004, pp. 1603-1609, pp 349-357.